



## Study on mechanism of photocatalytic performance of La-doped TiO<sub>2</sub>/Ti photoelectrodes by theoretical and experimental methods

Yanjun Xin <sup>a,\*</sup>, Huiling Liu <sup>b,\*</sup>

<sup>a</sup> School of Resource and Environment, Qingdao Agricultural University, Qingdao 266109, China

<sup>b</sup> State Key Laboratory of Urban Water Resources and Environment (SKLUWRE), Department of Environmental Science and Engineering, Harbin Institute of Technology, Huanghe Road 73, Nangang District, Harbin 150090, China

### ARTICLE INFO

#### Article history:

Received 3 May 2011

Received in revised form

27 August 2011

Accepted 10 October 2011

Available online 17 October 2011

#### Keywords:

Photoelectrocatalytic

La-doped TiO<sub>2</sub>

TiO<sub>2</sub> photoelectrode

First-principle

### ABSTRACT

TiO<sub>2</sub> photoelectrodes with various nanostructures have been successfully prepared by the anodization method. The morphology, microstructure and optical properties of as-prepared photoelectrodes were studied by scanning electron microscopy (SEM), X-ray diffraction (XRD), ultraviolet/visible light diffuse reflectance spectra (UV/vis/DRS), surface photovoltage spectroscopy (SPS) and photocurrent. The electronic structure and optical properties of La doped/undoped TiO<sub>2</sub> photoelectrodes with different crystal structures were calculated by the density function theory. The photocatalytic and photoelectrocatalytic activities of as-prepared photoelectrodes were evaluated. The results showed that the anodization potentials played a crucial role in the surface morphology and microstructure. Both results of theoretical calculations and experimental tests demonstrated that La-doped photoelectrodes were more sensitive to light than undoped one. The difference of photoelectrodes performance was ascribed to the crystal configuration, impurity energy levels and long-range orientation moving of photogenerated carriers.

© 2011 Elsevier Inc. All rights reserved.

### 1. Introduction

In the past three decades, TiO<sub>2</sub> photocatalysts have been extensively studied for water and wastewater treatment due to its optical and chemical stability, cheap, non-toxicity and no secondary pollution [1–5]. Unfortunately, TiO<sub>2</sub> photocatalyst can only be activated by UV radiation ( $\lambda < 380$  nm), which occupies only less than 5% of the solar irradiance at the Earth's surface [6]. For the sake of improving the utilization of sunlight, many methods have been studied, including transition metal and rare earth element doping [7,8], noble-metal deposition [9], non-metals doping [10–12], semiconductor coupled [13], sensitization [14,15], etc. [16]. Rare metals [17–20] have been widely used to improve the photocatalytic (PC) activity of TiO<sub>2</sub> photocatalysts, in order to expand the optical absorption range.

It was well known that Lanthanide ions could form complexes due to the interaction of various Lewis bases (e.g., acids, amines, aldehydes, alcohols, thiols, etc.), and the *f*-orbital of lanthanides, that could improve the adsorption of organic pollutants on catalyst surface [21,22]. Therefore, the incorporation of lanthanum into TiO<sub>2</sub> photocatalysts might facilitate to enhance the PC and photoelectrocatalytic (PEC) performance. Lanthanide-doped

nanoparticles have attracted extensive attention for their unique properties and prospective application in photocatalysis [21,23,24], optical materials [25] and photonic band gap materials [26]. Lanthanide-doped TiO<sub>2</sub> particles could be prepared by many methods, for example, sol-gel method [18,27], plasma spray method [28], sol-microwave method [29], hydrothermal method [30], magnetron sputtering method [31] and pulsed laser deposition [32]. However, little reports about the relation of microstructure and PC performance of La-TiO<sub>2</sub>/Ti photoelectrodes, in particular La-doped photoelectrodes, are prepared by the anodic oxidation technology.

In recent years, CASTEP codes based on density functional theory (DFT) were successfully used to study the crystal structure, electronic structure and optical properties [33,34]. So far, many researchers have carried out many investigations about TiO<sub>2</sub> photocatalyst by the density function theory [35], but few researchers focused on the relationship between crystal phases and PEC performance of La-TiO<sub>2</sub> photoelectrodes. In particular, to the best of our knowledge, there are no reports about the systematic investigation of the correlation between the band gap, optical properties and PC and PEC degradation rates of organic pollutants using La-TiO<sub>2</sub> photoelectrodes with different crystal structures. To fundamentally understand such structure–activity relationships, it was important to provide deep insights into the microstructure and PC and PEC activities of La-doped/undoped TiO<sub>2</sub> photoelectrodes.

In present research, La-TiO<sub>2</sub> photoelectrodes were successfully fabricated by the anodic oxidation method in La(NO<sub>3</sub>)<sub>3</sub> solution. The crystal structure, electronic structure, optical properties and

\* Corresponding authors.

E-mail addresses: xintom770824@yahoo.com.cn (Y. Xin), hliu2002@163.com (H. Liu).

photocatalysis performance were systematically investigated by the theoretical and experimental methods. The effect of La ion on the structure–activity relationships of La-TiO<sub>2</sub> photoelectrodes was discussed. It would be a potential method for practical application in environmental sciences and mechanism analysis of PC and PEC properties of modified TiO<sub>2</sub>/Ti photoelectrodes.

## 2. Experimental methods

### 2.1. Chemicals and materials

Titanium (Ti) foils (purity > 99.7%, 0.2 mm thickness) were purchased from Baoji Titanium and Nickel Manufacture Limited Company, China. Other chemicals were obtained as analytical reagent grade and used without further purification. The sample solutions were prepared with deionized water.

### 2.2. Sample preparation and characterization

Pure TiO<sub>2</sub>/Ti photoelectrodes were fabricated in a dual-electrode reaction chamber, in which the cleaned Ti sheet and copper foil of the same size were used as the anode and cathode, respectively. Two electrodes with a distance of 3 cm were submerged in 0.5 mol/L H<sub>2</sub>SO<sub>4</sub> solution. Current density of 100 mA/cm<sup>2</sup> was provided from the beginning of the oxidation reaction until the voltage reached the determined value (120 V, 160 V and 200 V). The total reaction time was 10 min. The samples were immediately rinsed with deionized water and dried in 378 K for 30 min. La-TiO<sub>2</sub> photoelectrodes were fabricated using the same method in the mixed solution of 0.5 mol/L H<sub>2</sub>SO<sub>4</sub> and 1 g/L La(NO<sub>3</sub>)<sub>3</sub>. La-doped and undoped TiO<sub>2</sub>/Ti photoelectrodes prepared in different voltage were labeled as La-120, La-160, La-200, P-120, P-160 and P-200 (the number denoted the voltage).

Surface morphology of as-prepared photoelectrodes was studied by the scanning electronic microscopy (SEM, S-4700-Japan). Crystal structure was examined using a D/max-rB X-ray diffraction (XRD) with CuK $\alpha$  radiation ( $\lambda=1.54050$ ). Measurements were performed at 0.02° intervals of  $2\theta$  over the range of 10–90°. The composition and bonding energy of La ion on the surface of the films were detected by an X-ray photoelectron spectroscopy (XPS, PHI 5700 ESCA system spectrometer) using AlK $\alpha$  X-ray (1486.6 eV) at 15 kV and 100 W. The binding energy was referenced to the C1s peak at 284.8 eV for calibration. Diffuse reflectance spectra (DRS) were recorded using a Lambda 900 UV-vis spectrophotometer (Perkin Elmer Company) with a diffuse reflectance accessory. The surface photovoltage spectroscopy (SPS) was tested in Jilin University. Photocurrent was investigated using the CHI EC analyzer (a Model 263A Potentiostat/Galvamastat, America) in standard three-electrode system. TiO<sub>2</sub> photoelectrode, Pt foil and a saturated calomel electrode (SCE) were used as photo-anode, counter electrode and the reference electrode, respectively. 35 W Xenon light, which mainly provided light wavelength in 380–800 nm, was used as artificial solar light. All experiments were performed at 298 K.

### 2.3. PC and PEC activity evaluation

PC and PEC performance of as-prepared photoelectrodes were evaluated by discoloration rate of Rhodamine B (Rh.B) in a single-compartment cylindrical quartz reactor. The photoelectrode with an active area of 2.5 cm<sup>2</sup> is immersed in 5 mg/L Rh.B solution. Prior to illumination, the sample solution was stirred for 30 min in dark to reach the adsorption/desorption equilibrium. The concentrations of Rh.B were analyzed by the UV/Vis spectrophotometer (UV2500, SHIMADZU).

### 2.4. Calculation details

All calculations were carried out by CASTEP code, which was based on the density functional theory (DFT) approach. The exchange and correlation interactions were modeled using the generalized gradient approximation (GGA), together with the Perdew–Burke–Ernzerhof (PBE) [33,35] exchange–correlation functional and ultrasoft pseudopotentials. The core electrons were replaced by the ultrasoft core potentials, and the valence atomic configurations were 3p<sup>6</sup>3d<sup>2</sup> 4s<sup>2</sup> for Ti, 2s<sup>2</sup>2p<sup>4</sup> for O and 5p<sup>6</sup>5d<sup>1</sup>6s<sup>2</sup> for La.

For the sake of comparison, 48-atom supercells were used to construct all calculation models. One titanium atom in the supercell was replaced by a lanthanum atom for La-doped TiO<sub>2</sub> model. The cut-off energy of 340 eV and a 3 × 3 × 3  $k$ -point set centered at point are sufficient to make the total energy converge to within a tolerance of 10<sup>−6</sup> eV/atom. The lattice parameters and the atomic positions were fully optimized until all components of the residual forces were smaller than 0.05 eV/Å.

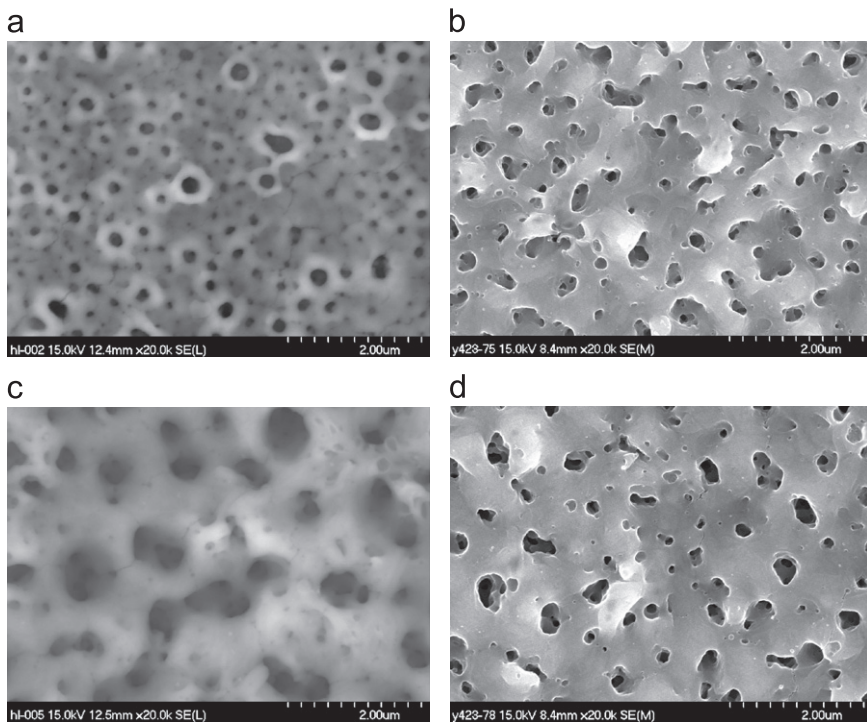
In order to compare conveniently the band structure and optical property of La-doped and undoped TiO<sub>2</sub> photoelectrodes, the same optimization and calculation conditions were used. “Scissors operators” [36] were introduced to shift all the conduction levels to meet with the measured value (3.2 eV for anatase TiO<sub>2</sub> and 3.0 eV for rutile TiO<sub>2</sub>). A rigid “scissor operator” correction of 1.0 eV was applied for anatase TiO<sub>2</sub> (P-120 and La-120) photoelectrodes and 1.1 eV was applied for rutile TiO<sub>2</sub> (P-200 and La-200) photoelectrodes in order to keep consistency with the experimental value.

## 3. Results

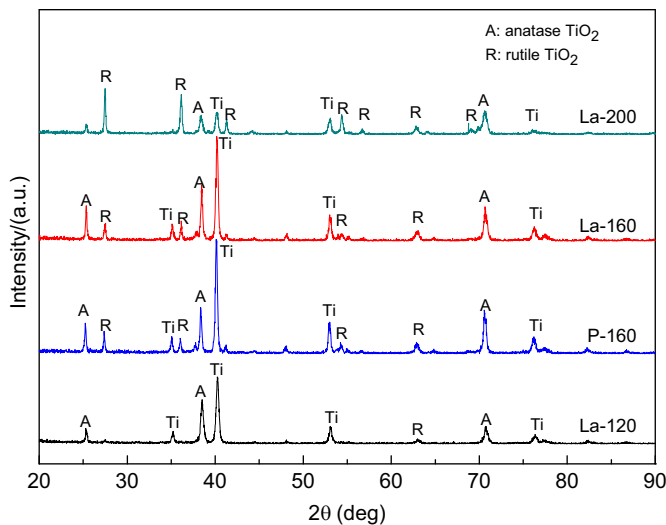
### 3.1. Morphology and structure characterization

Fig. 1 showed the morphology of as-prepared photoelectrodes. The average aperture of La-120, La-160 and La-200 photoelectrodes were ~90 nm, ~200 nm and ~500 nm, which were similar to P-120, P-160 and P-200 photoelectrodes, respectively (the latter were not shown). The results showed that the samples have rough and porous surface and the average aperture increased with the voltage.

The results in Fig. 2 showed XRD patterns of as-prepared photoelectrodes (the XRD pattern of P-120 photoelectrodes was similar with La-120 photoelectrodes, also P-200 and La-200 photoelectrodes). The results in Fig. 2 indicated that the fraction of rutile TiO<sub>2</sub> increased with the voltage, and the crystal structures of La-120 were mainly composed of anatase TiO<sub>2</sub>, while La-200 photoelectrodes were mainly composed of rutile TiO<sub>2</sub>. So La-120 was used to stand for La-doped anatase TiO<sub>2</sub> models and La-200 was used to represent La-doped rutile TiO<sub>2</sub> models. P-120 and P-200 stand for pure anatase and rutile TiO<sub>2</sub> model, respectively. According to the characteristic peaks, both La-160 and P-160 photoelectrodes were composed of mixed anatase and rutile TiO<sub>2</sub>; however, the fraction of rutile TiO<sub>2</sub> in La-160 photoelectrodes was lower than that in P-160 photoelectrodes. For the mixed crystal photoelectrodes, the fraction of rutile TiO<sub>2</sub> could be estimated according to the literature [28]. The calculation results showed that the fraction of rutile TiO<sub>2</sub> in La-160 photoelectrodes was 38%, while that in P-160 photoelectrodes was 45%. The results indicated that La doping inhibited the transformation of anatase TiO<sub>2</sub> to rutile phase TiO<sub>2</sub> [27]. The XPS results in Fig. 3 showed that the lanthanum does exist in the La-doped TiO<sub>2</sub> photocatalysts as oxides La<sub>2</sub>O<sub>3</sub>. The binding energy of 835.1 eV and 852.7 eV corresponded to La3d<sub>5/2</sub> and La3d<sub>3/2</sub> energy level, respectively. At the interface, titanium atom might substitute lanthanum atom in the lattice of La<sub>2</sub>O<sub>3</sub> alternatively, and a Ti–O–La bond could be formed.



**Fig. 1.** SEM of La-doped and undoped  $\text{TiO}_2$  photoelectrodes prepared at different voltages. (a) La-120, (b) La-160, (c) La-200 and (d) P-160.



**Fig. 2.** XRD patterns of La-doped and undoped  $\text{TiO}_2$  photoelectrodes prepared at different voltages.

### 3.2. Band structure and optical absorption properties

In order to elucidate the roles of crystal structure and La ion in  $\text{TiO}_2$  photoelectrodes, we calculated the electronic structures and optical properties of P-120, P-200, La-120 and La-200 photoelectrodes. The curves of them were plotted in Figs. 4 and 5.

The results in Fig. 4 showed that P-200 photoelectrode has a direct gap at G point, while P-120 photoelectrode has an indirect one between G and F, which were in accordance with the previously reported results [33]. The results also showed that La-200 photoelectrode has a direct gap at G point and La-120 photoelectrode has an indirect one between G and Z. For La-120 and La-200 photoelectrodes, the band gap narrowed to 0.3 eV and 0.2 eV comparing with their undoped photoelectrodes, respectively. On La- $\text{TiO}_2$  photoelectrodes their 4f and 5d states formed

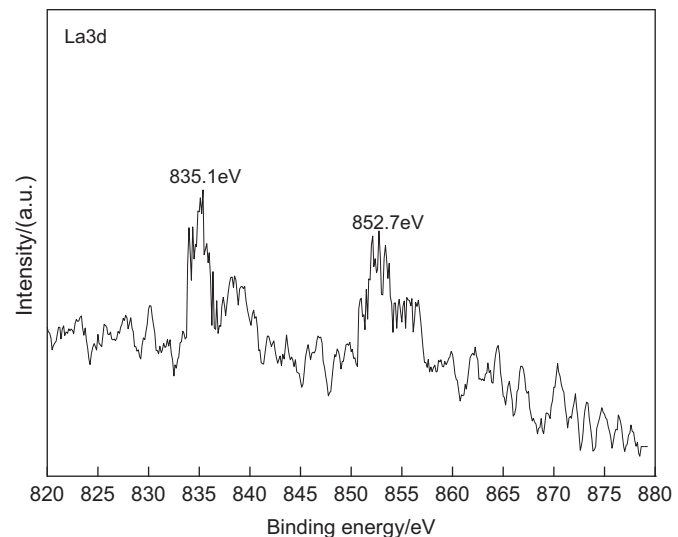


**Fig. 3.** XPS spectra of La in La- $\text{TiO}_2$  photoelectrodes.

the impurity energy levels (IELs). The IELs did not occur in the middle of band gap like nonmetal-doped  $\text{TiO}_2$ , while located at the middle of CB and VB [37]. So the width of CB and VB were broadened and the band gap of La- $\text{TiO}_2$  photoelectrode became narrower. Thus the absorption edges of  $\text{TiO}_2$  photoelectrode would red-shift toward visible-light region. Another important feature was that Fermi level crossed the top of VB, so it was not fully filled with electrons at the ground state.

Optical properties of P-120, P-200, La-120 and La-200 photoelectrodes were plotted in Fig. 5. The results demonstrated that La-120 and La-200 photoelectrodes showed a little red-shift to 400 nm comparing with P-120 and P-200 photoelectrodes, respectively. The absorption coefficient of P-200 photoelectrode was higher than that of P-120 photoelectrodes in the whole light spectrum. It was interesting that the absorption coefficient of La-200

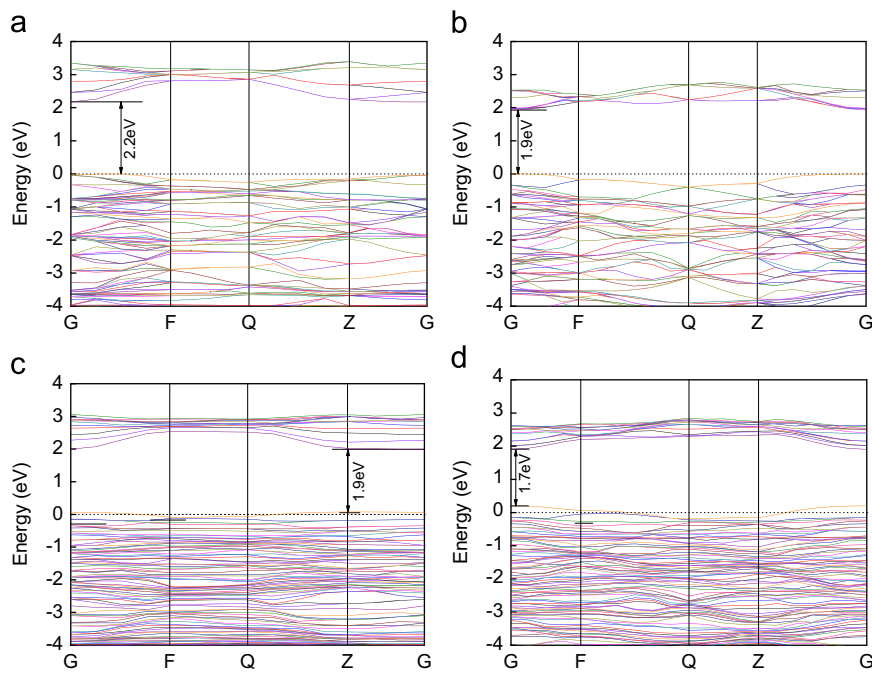


Fig. 4. Band structure of P-120, P-200, La-120 and La-200 photoelectrodes.

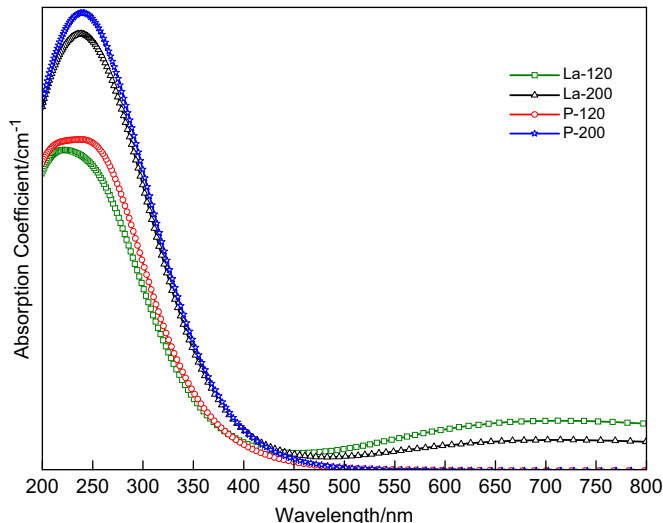


Fig. 5. Optical absorption curves of P-120, P-200, La-120 and La-200 photoelectrodes.

photoelectrode was higher than that of La-120 photoelectrode in ultraviolet region, but it was reverse in visible region. The results in Fig. 4 indicated that La-doped  $\text{TiO}_2$  photoelectrodes were more sensitive to light than that of the undoped one. The photoresponse would be another important factor to influence the results of UV/vis/DRS, SPS and photocurrent of  $\text{TiO}_2$  photoelectrodes, as well as PC and PEC activity. In order to verify the theoretical analysis results, the optical properties and PC activity of La-doped and undoped photoelectrodes were carried out by experimental tests in the later part.

### 3.3. Optical and photoelectrochemical properties

The optical and photoelectrochemical properties are regarded as key parameters to characterize the photoactivities and the photoelectrochemical properties. UV/vis/DRS and SPS could detect optical absorption property due to the drift, accumulation and recombination

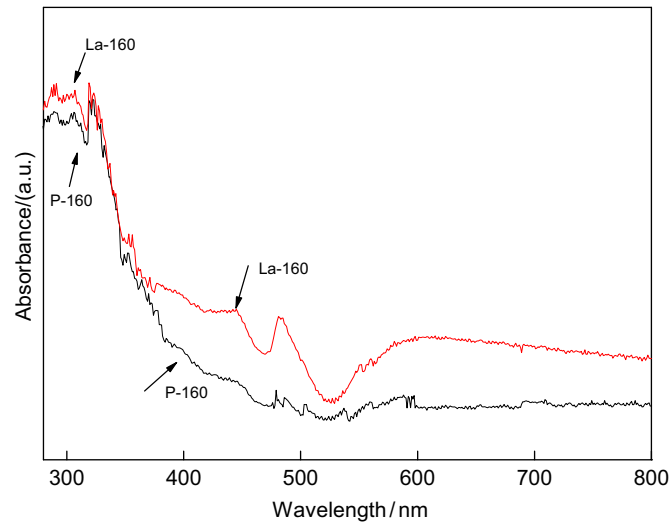


Fig. 6. UV-vis DRS spectra of P-160 and La-160  $\text{TiO}_2/\text{Ti}$  photoelectrodes.

of photogenerated carriers. The photocurrent could show the properties of light-induced charge transfer between the electrode and solution interface. The results of UV/vis/DRS, SPS and photocurrent were presented in Figs. 6–8.

The results of UV/vis/DRS in Fig. 6 shows that in the whole light region, the absorption intensity of La-160 photoelectrode was stronger than P-160 photoelectrode, which indicated that La-doped  $\text{TiO}_2$  photoelectrode was more sensitive to solar light than undoped one. In the meantime, a shift of the absorption threshold toward the visible region was observed for La-160 photoelectrode. The SPS results in Fig. 7 shows that La-160 photoelectrode displayed stronger SPS signal than that of P-160 photoelectrode in ultraviolet and visible region. The results of photocurrent-time curves in Fig. 8 verified that La doped photoelectrode have higher transfer efficiency of the photogenerated electrons. All the results of Figs. 6–8 corresponded to the theoretical calculation result shown in Figs. 4 and 5.

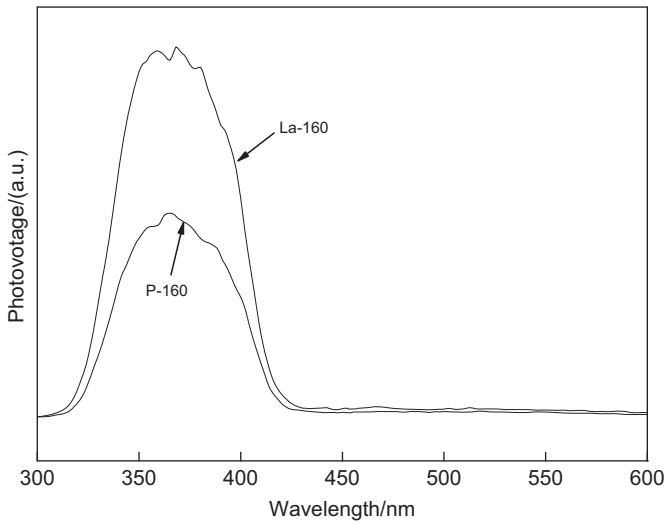


Fig. 7. SPS spectra of P-160 and La-160  $\text{TiO}_2/\text{Ti}$  photoelectrodes.

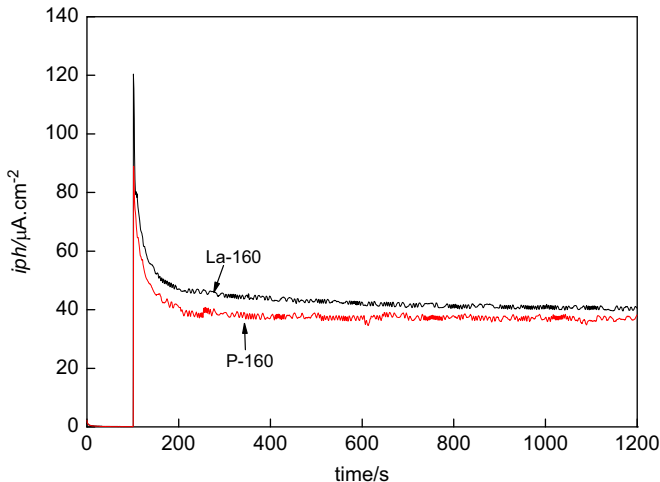


Fig. 8. Photocurrent of P-160 and La-160  $\text{TiO}_2/\text{Ti}$  photoelectrodes in 0.5 mol/L  $\text{Na}_2\text{SO}_4$  solutions.

The results in Figs. 6–8 showed that the conclusions of UV/vis/DRS, SPS and photocurrent were consistent and La ion would improve light response of  $\text{TiO}_2$  photoelectrodes. All conclusions implied that La ion in the lattice of  $\text{TiO}_2$  facilitated to improve PC and PEC activities of  $\text{TiO}_2$  photoelectrodes.

#### 3.4. Evaluation of PC and PEC activity

The results in Fig. 9 showed Rh.B discoloration rate as a function of time of La-120, La-160, La-200, P-120, P-160 and P-200 photoelectrodes. The results showed that all photodiscoloration rates increased gradually with the increase of illumination time. After 120 min Rh.B photodiscoloration rates of La-120, La-160, La-200, P-120, P-160 and P-200 photoelectrodes were 22.5%, 53.7%, 42.4%, 20.1%, 45.7% and 23.7%, respectively. The photodiscoloration rate of La-200 photoelectrode increased about 19% than that of P-200 photoelectrode, and that of La-160 photoelectrode was 8% higher than P-160 photoelectrode. The results showed that La doping could improve PC activity of as-prepared photoelectrodes. The results in Fig. 9 also show that Rh.B photodiscoloration rates of La-160 and P-160 photoelectrodes were higher than that of La-120, La-200, P-120 and P-200 photoelectrodes. When the optimized assistant potential of 1.0 V

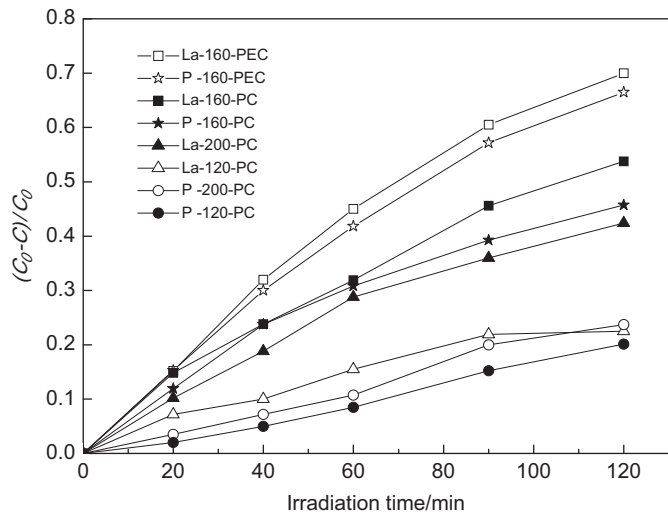


Fig. 9. Rh.B discoloration rates of La-doped/undoped  $\text{TiO}_2/\text{Ti}$  photoelectrodes.

was applied, Rh.B photodiscoloration rates of La-160 and P-160 photoelectrodes achieved 70% and 66.5% after 120 min, and the photodiscoloration rate enhanced by 16.3% and 20.8% than that of no assistant potentials, respectively. In the meantime, the difference of Rh.B photodiscoloration rates between La-160 and P-160 photoelectrodes changed from 8% to 3.5% after the assistant potential was applied. In general, the trend of photodiscoloration rates of Rh.B as a function of time was La-160-PEC > P-160-PEC > La-160 > P-160 > La-200 > La-120 ≈ P-200 > P-120.

#### 4. Discussions

The results of PC and PEC experiments showed that Rh.B discoloration rates of as-prepared photoelectrodes presented significant difference. In order to provide deep insights into the diversity, the crucial factors in details were elucidated based on our results.

Many researchers believed that the incorporation of lanthanide ions into  $\text{TiO}_2$  lattice could provide a larger specific surface area [24,30] and concentrate organic pollutant [27] at the semiconductor surface than pure one, which might lead to excellent physicochemical properties and catalytic behavior. However, our adsorption experiments indicated that the adsorptions of Rh.B (not given in the paper) on La-doped and undoped  $\text{TiO}_2$  photoelectrodes have no obvious difference. Thus, in our experiments the difference of adsorptions was not crucial factor on PC and PEC activity.

Xu et al. [28] and He et al. [38] thought that it was difficult, even impossible [39], for La ion to replace Ti ion in the lattice of  $\text{TiO}_2$ , because the ionic radius of La ion (0.106 nm) was much larger than that of Ti ion (0.068 nm), thus La ion was mainly present in the surface layer of  $\text{TiO}_2$ . The results might be attributed to the specific synthesis route that their La- $\text{TiO}_2$  catalysts were fabricated by  $\text{TiO}_2$  supported Lanthanum compounds and followed by sintering. Under such a moderate multi-step method the La ion would difficultly, even impossibly transfer from the interface into the lattice of bulk  $\text{TiO}_2$  to replace Ti ion. Though the radius of La ion is much larger than Ti ion (0.068 nm), it is still smaller than oxygen (0.14 nm). Hence according to the literatures [18,27] and the rule of similarity, under suitable conditions, i.e. in high temperature or high voltage, La ion could enter into  $\text{TiO}_2$  lattice to substitute for Ti ion evenly and could form Ti–O–La bond [27,38] and form limited solid solutions. In our experiments,  $\text{TiO}_2$  photoelectrodes were fabricated in  $\text{La}(\text{NO}_3)_3$  electrolytes by the one-step anodization method. Under

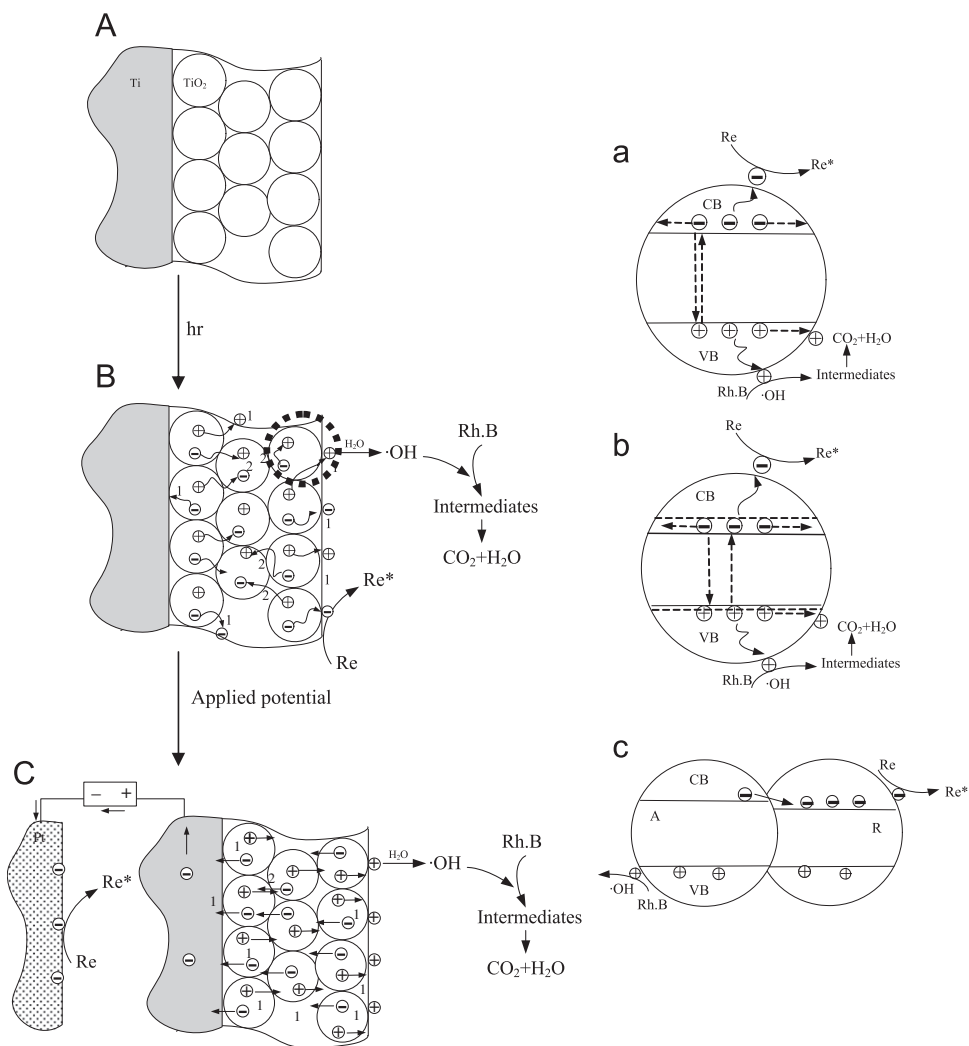
located high temperature originated from high voltage, La ion would smoothly enter into the interior of  $\text{TiO}_2$  film rather than only located at the two interfaces. Thus the replacement of Ti ion in the lattice of  $\text{TiO}_2$  would be accessible. In XRD results the crystal of  $\text{La}_2\text{O}_3$  were not detected, while our X-ray photoelectron spectroscopy demonstrated the presence of La ion. The absence of crystalline La and lanthanide oxide phase might be due to the incorporation into  $\text{TiO}_2$  lattice and formed Ti–O–La bonds. It was known that  $\text{La}_2\text{O}_3$  showed no PC activity [18], however in our experiments all UV/vis/DRS, SPS and photocurrent test verified that La– $\text{TiO}_2$  photoelectrodes have superior performance than undoped one. These results indicated that Ti–O–La bonds might have been formed at the interface.

The La ion in the Ti–O–La bond would disturb the charge balance, which would influence the surface chemical state of La– $\text{TiO}_2$  photoelectrodes. The charge imbalance, caused by the difference of valence state, could facilitate hydroxide ions to adsorb on the surface [30], which could accept holes generated by irradiation, and form hydroxyl radicals. Therefore, the recombination of photoinduced charges could be suppressed. At the same time, the modification of  $\text{La}^{3+}$  would provide a limited amount of  $\text{O}_2^-$  and  $\text{Ti}^{3+}$  species, which could trap photogenerated holes, on the surface or in bulk  $\text{TiO}_2$ .  $\text{Ti}^{4+}$  species and

surface oxygen vacancy could trap photogenerated electrons and formed  $\text{Ti}^{3+}$  and anions  $\text{O}_2^-$ , respectively [22,30]. The capture of carriers could prolong their lifetime and inhibit the recombination of photogenerated electron–hole pairs, thus enhanced PC and PEC activity of La– $\text{TiO}_2$  photoelectrodes.

According to XRD patterns, the content of rutile  $\text{TiO}_2$  in La– $\text{TiO}_2$  photoelectrodes increased from 0% to 94% in company with the voltage changed from 120 V to 200 V, which were different from other conclusions that the crystal structures were mainly composed of anatase phase even in the high temperature of 800 K [5]. Furthermore, the anodization voltage played a crucial role in crystal structures of  $\text{TiO}_2$  photoelectrodes and could alter crystal phase from anatase  $\text{TiO}_2$  to rutile  $\text{TiO}_2$ . It was well known that the band gap of rutile  $\text{TiO}_2$  was narrower than that of anatase  $\text{TiO}_2$ . Therefore, the photoresponse of rutile  $\text{TiO}_2$  could be stronger than that of anatase  $\text{TiO}_2$  under artificial solar light, which was responsible for the higher discoloration rate of La–200 photoelectrode than that of La–120 photoelectrode, and also that of P–200 photoelectrode and P–120 photoelectrodes.

As deduced from XRD spectra of La–160 and P–160 photoelectrodes, the fraction of rutile  $\text{TiO}_2$  in La–160 photoelectrodes



**Scheme 1.** Mechanism of photophysical chemistry processes in as-prepared  $\text{TiO}_2$  photoelectrodes. The overall scheme of  $\text{TiO}_2$  photoelectrodes: (A) microstructure of  $\text{TiO}_2$  photoelectrodes; (B) movement of photoelectrons and holes without bias potentials; (C) movement of photoelectrons and holes at applied bias potentials; (a), (b) and (c) were the transmission of photogenerated electrons and holes of local enlargement of (B) (dot line circle): (a) photoelectrons movement in P-120 (anatase  $\text{TiO}_2$ ) and P-200 (rutile  $\text{TiO}_2$ ) photoelectrodes; (b) photoelectrons movement in La-120 (anatase  $\text{TiO}_2$ ) and La-200 (rutile  $\text{TiO}_2$ ) photoelectrodes, the dot line denotes the top of valence band (VB) and the bottom of conduction band (CB) of pure photoelectrodes; (c) photoelectrons movement in P-160 and La-160  $\text{TiO}_2$  photoelectrodes (mixed crystal phase). The number refers to as follows: (1) transmission process of photoelectrons and holes; (2) recombination process of photoelectrons and holes. Arrows represent the moving direction of photoelectrons.

decreased from 45% to 38% due to the effect of La ion in the lattice of  $\text{TiO}_2$ . The results indicated that La ion inhibited the transformation from anatase to rutile  $\text{TiO}_2$  [8]. For La ion was more electropositive than Ti ion, it would render its electronic concentration to  $\text{O}_2^-$  and strengthen the Ti–O bond between the less electropositive  $\text{Ti}^{4+}$  ions. Thus the Ti–O bond would be difficult to break than that of pure one, and the A–R transition was retarded. Our conclusions were in general agreement with the literature reports [8,27], except that the rutile  $\text{TiO}_2$  still accounted for a large proportion in our sample. The mixed crystal structure would constitute self-semiconductor coupling effect, which could promote the separation efficiency of photogenerated electrons–holes pairs, and then produced much more oxygen species to improve PC activity of La-160 and P-160 photoelectrodes. The co-effect of self-coupling effect and La ion made La-160 photoelectrodes have highest discoloration rate in as-prepared photoelectrodes. When assistant potential was applied, the moving direction of photogenerated electrons and holes altered from random to long-range orientation under the influence of electric field, which decreased greatly the recombination opportunities of them. So Rh.B discoloration rates of La-160 and P-160 photoelectrodes would be improved.

Taking into account the former results, the effect of La IELs, self-semiconductor coupling and long-range orientation of photogenerated carriers originated from applied electric field would be responsible for the trend of PC and PEC activity of as-prepared  $\text{TiO}_2$  photoelectrodes. The possible transmission of photogenerated charges and degradation pathway of Rh.B could be summarized in **Scheme 1**. La IELs reduced the band gap of La-120, La-160 and La-200 photoelectrodes (**Scheme 1(a)** and (**b**)) and improved photoresponse in visible light, thus PC activities were promoted. The mixed crystal structure could facilitate the separation of photogenerated electrons and holes due to the self-semiconductor coupling effect (**Scheme 1(c)**), which was responsible for the higher PC performance of P-160 photoelectrode. La-160 photoelectrode has the highest photodiscoloration rate of Rh.B in all as-prepared photoelectrodes due to the cooperation of band gap narrowing, enhanced photoresponse and mixed crystal structure. When there was no applied potentials La IELs and self-coupling effect were responsible for the separations of photogenerated charges. When the assistant potential was applied the moving direction of photogenerated electrons and holes would alter from random to orientation under the effect of electric field (**Scheme 1(A)–(C)**), thus the recombination opportunities of photogenerated carriers were reduced greatly. In conclusion, the effects of the former reasons were responsible for the discrepancy of PC and PEC performance of La-120, La-160, La-200, P-120, P-160 and P-200 photoelectrodes.

## 5. Conclusions

In this study, La-120, La-160, La-200, P-120, P-160 and P-200 photoelectrodes have been successfully prepared by the one-step anodization method. Voltage was a crucial factor in the crystal structure. La-doped  $\text{TiO}_2$  photoelectrodes have a narrower band gap and could improve photoresponse of  $\text{TiO}_2$  photoelectrode in visible light. La-IELs, anatase/rutile self-coupling effect and assistant potential could promote the separation efficiency of photogenerated electrons and holes.

## Acknowledgment

This work was supported by National Natural Science Foundation of China (no. 51178138), National Creative Research Groups of National Natural Science Foundation of China (no. 50821002) and State Key Laboratory of Urban Water Resources and Environment (no. 2010DX03).

## References

- [1] K. Vinodgopal, S. Hotchandani, P.V. Kamat, *J. Phys. Chem.* 97 (1993) 9040–9044.
- [2] O.M. Alfano, D. Bahnemann, A.E. Cassano, R. Dillert, R. Goslich, *Catal. Today* 58 (2000) 199–230.
- [3] R.J. Candal, W.A. Zeltner, M.A. Anderson, *Environ. Sci. Technol.* 34 (2000) 3443–3451.
- [4] M.E. Calvo, R.J. Candal, S.A. Bilmes, *Environ. Sci. Technol.* 35 (2001) 4132–4138.
- [5] X.Z. Li, H.S. Liu, *Environ. Sci. Technol.* 39 (2005) 4614–4620.
- [6] R. Asahi, T. Morikawa, T. Ohwaki, K. Aoki, Y. Taga, *Science* 293 (2001) 269–271.
- [7] H.S. Peng, S.H. Huang, F.T. You, J.J. Chang, S.Z. Lu, L. Cao, *J. Phys. Chem. B* 109 (2005) 5774–5778.
- [8] C.P. Sibu, S.R. Kumar, P. Mukundan, K.G.K. Warrier, *Chem. Mater.* 14 (2002) 2876–2881.
- [9] J.G. Yu, J.F. Xiong, B. Cheng, S.W. Liu, *Appl. Catal. B-Environ.* 60 (2005) 211–221.
- [10] K.M. Parida, N. Sahu, A.K. Tripathi, V.S. Kamble, *Environ. Sci. Technol.* 44 (2010) 4155–4160.
- [11] L. Han, Y.J. Xin, H.L. Liu, X.X. Ma, G.Z. Tang, *J. Hazard. Mater.* 175 (2010) 524–531.
- [12] Z.P. Wang, W.M. Cai, X.T. Hong, X.L. Zhao, F. Xu, C.G. Cai, *Appl. Catal. B-Environ.* 57 (2005) 223–231.
- [13] W.T. Sun, Y. Yu, H.Y. Pan, X.F. Gao, Q. Chen, L.M. Peng, *J. Am. Chem. Soc.* 130 (2008) 1124–1128.
- [14] J.M. Macak, H. Tsuchiya, A. Ghicov, P. Schmuki, *Electrochem. Commun.* 7 (2005) 1133–1137.
- [15] G. Mele, E. Garcia-Lopez, L. Palmisano, G. Dyrda, *J. Phys. Chem. C* 111 (2007) 6581–6588.
- [16] Y.B. Xie, X.Z. Li, *J. Hazard. Mater.* 138 (2006) 526–533.
- [17] Y.B. Xie, C.W. Yuan, *Appl. Catal. B-Environ.* 46 (2003) 251–259.
- [18] Y.H. Zhang, H.X. Zhang, Y.X. Xu, Y.G. Wang, *J. Solid State Chem.* 177 (2004) 3490–3498.
- [19] S.J. Pang, X.L. Li, G. Yang, Z.S. Shi, Y. Wan, Z.C. Cui, *J. Mater. Sci.* 45 (2010) 2359–2364.
- [20] J. Choi, H. Park, M.R. Hoffmann, *J. Phys. Chem. C* 114 (2010) 783–792.
- [21] K.T. Ranjit, I. Willner, S.H. Bossmann, A.M. Braun, *J. Catal.* 204 (2001) 305–313.
- [22] K.T. Ranjit, I. Willner, S.H. Bossmann, A.M. Braun, *Environ. Sci. Technol.* 35 (2001) 1544–1549.
- [23] K.T. Ranjit, H. Cohen, I. Willner, S. Bossmann, A.M. Braun, *J. Mater. Sci.* 34 (1999) 5273–5280.
- [24] J.J. Xu, Y.H. Ao, D.G. Fu, C.W. Yuan, *J. Hazard. Mater.* 164 (2009) 762–768.
- [25] A.L. Linsebigler, G.Q. Lu, J.T. Yates, *Chem. Rev.* 95 (1995) 735–758.
- [26] J.D. Joannopoulos, P.R. Villeneuve, S.H. Fan, *Nature* 386 (1997) 143–149.
- [27] F.B. Li, X.Z. Li, M.F. Hou, *Appl. Catal. B-Environ.* 48 (2004) 185–194.
- [28] D.P. Xu, L.J. Feng, A.L. Lei, *J. Colloid Interface Sci.* 329 (2009) 395–403.
- [29] A.F. Shoaie, M.H. Loghmani, *Chem. Eng. J.* 157 (2010) 263–269.
- [30] T.Y. Peng, D. Zhao, H.B. Song, C.H. Yan, *J. Mol. Catal. a-Chem.* 238 (2005) 119–126.
- [31] K. Zatkrewska, M. Radecka, A. Kruk, W. Osuch, *Solid State Ionics* 157 (2003) 349–356.
- [32] M.P. Besland, H.D.A. Aissa, P.R.J. Barroy, S. Lafane, P.Y. Tessier, B. Angleraud, M. Richard-Plouet, L. Brohan, M.A. Djouadi, *Thin Solid Films* 495 (2006) 86–91.
- [33] F. Labat, P. Baranek, C. Domain, C. Minot, C. Adamo, *J. Chem. Phys.* 126 (2007) 154703/1–12.
- [34] K.S. Yang, Y. Dai, B.B. Huang, M.H. Whangbo, *Phys. Chem. C* 113 (2009) 2624–2629.
- [35] E. Finazzi, C. Di Valentin, A. Selloni, G. Pacchioni, *J. Phys. Chem. C* 111 (2007) 9275–9282.
- [36] R.W. Godby, M. Schluter, L.J. Sham, *Phys. Rev. B* 37 (1988) 10159–10175.
- [37] Z.Y. Zhao, Q.J. Liu, *J. Phys. D-Appl. Phys.* 41 (2008) 085417.
- [38] Z.Q. He, X. Xu, S. Song, L. Xie, J.J. Tu, J.M. Chen, B. Yan, *J. Phys. Chem. C* 112 (2008) 16431–16437.
- [39] T.D. Nguyen-Phan, M.B. Song, E.J. Kim, E.W. Shin, *Micropor. Mesopor. Mater.* 119 (2009) 290–298.